Proceedings of the ASME 2023 42nd International Conference on Ocean, Offshore and Arctic Engineering
OMAE2023
June 11-16, 2023, Melbourne, Australia

OMAE2023-102788

DYNAMIC POWER CABLE CONFIGURATION DESIGN FOR FLOATING OFFSHORE WIND TURBINES USING GRADIENT-BASED OPTIMIZATION

Anja Schnepf
Department of Mechanical and Structural Engineering and Materials Science
University of Stavanger
CoreMarine
Stavanger, Norway

Knut Erik Teigen Giljarhus
Department of Mechanical and Structural Engineering and Materials Science
University of Stavanger
Stavanger, Norway

Øyvind Johnsen
CoreMarine
Oslo, Norway

Carlos Lopez-Pavon
CoreMarine
Madrid, Spain

ABSTRACT

Power cables transmit the electric energy generated by offshore wind turbines to consumers on land and at sea. The power cables usually lie statically on the seabed to prevent them from moving and being damaged. Since floating offshore wind turbines (FOWTs) are positioned using mooring systems, their power cables are placed from a hang-off location at the floater through the water to the seabed. In this dynamic section, they must withstand environmental loads and the loads induced by the FOWT motions. A minimized power cable length is crucial for low transmission losses during operation, which is a priority during the design of the overall configuration. This work presents a dynamic power cable configuration modeling approach using gradient-based optimization. The applied method is Sequential Least Squares Programming (SLSQP). Its applicability is shown in the example optimization of a tethered lazy-wave dynamic power cable configuration connected to a spar-FOWT. The optimization method is applied with two and three design variables. Steady-state analyses with extreme environmental loads are performed at each iteration, considering three distinct loading directions. The resulting optimized power cable configurations have a shorter cable length than the initial configurations. Dynamic analyses of the optimized configuration show that it satisfies the design limits.

Keywords: optimization, dynamic cable configuration, umbilical, power cable, floating offshore wind turbine

1. INTRODUCTION

The design of inter-array power cable configurations in floating offshore wind parks is crucial for the transmission of the electrical energy generated by the FOWT to a consumer. In wind farms with fixed turbine foundations, the power cables lay on the seabed or are buried to avoid the impact of dynamic environmental loads [1]. The station-keeping of a FOWT is achieved via mooring lines, and the power cable cannot be placed on the seabed directly. Hence, it is placed from a hang-off location at the floater through the water to the seabed. In this section, the power cable experiences dynamic loads from the environment and the FOWT motions. Three main dynamic power cable configurations have been researched until today. First, in a design known as the catenary configuration, the power cable hangs freely between the floater and the seabed. Second, buoyancy modules are attached to the power cable at different locations in the lazy-wave configuration. Third, the tethered lazy-wave configuration is similar to the lazy-wave configuration, with the addition of an anchored tether attached to the cable near the TDP. It is also named a reverse pliant wave configuration. The latter two configuration types are the most common in offshore applications. They are used in the existing floating offshore wind farms Hywind Scotland [2], WindFloat Atlantic [3], and Hywind Tampen [4]. Rentschler et al. [5] performed static analyses to compare lazy-wave and catenary power cable configurations connected to a FOWT in shallow and

intermediate water depths. Regarding cable tension and curvature, the lazy-wave configuration performed better than the catenary configuration. A lazy-wave and a double-wave power cable configuration connected to a FOWT in shallow water were studied by Zhao et al. [6]. The double-wave configuration has two buoyancy sections, unlike the lazy-wave configuration with a single buoyancy section. The double-wave power cable configuration was proven more suitable in shallow waters because it has lower stresses, less curvature, and a longer fatigue life than the lazy-wave configuration. Ikhennicheu et al. [7] reported on the existing designs of offshore dynamic cable configurations.

In addition to floating offshore wind farms, various other uses of lazy-wave umbilical and power cable configurations have been described. Ottesen [8] described a deepwater application for a lazy-wave-shaped umbilical in a water depth of 1300 m and carried out dynamic simulations. He demonstrated a correlation between the axial velocity at the hang-off and the tensions in the sag where the buoyancy modules are attached. Dynamic simulations of a cable umbilical connected to a static wave energy converter (WEC) were carried out by Hall et al. [9]. They validated their lumped-mass line-dynamic model MoorDyn by comparing the lazy-wave simulation results with those obtained from the program OrcaFlex. Nicholls-Lee et al. [10] evaluated experimental and numerical results from a lazy-wave power cable configuration in shallow water depth connected to a buoy. They concluded that the bending stiffness of the cable is a crucial parameter for the behavior of the cable. The current intensity and direction are the most critical design considerations according to the results obtained from Thies et al. [11] in steady-state analyses of a shallow water lazy-wave configuration connected to a WEC. Thies et al. [12] studied a dynamic power cable attached to a WEC in shallow water. They concluded that the lazy-wave configuration has lower maximum stresses and a much longer fatigue life than the catenary configuration. Martinelli et al. [13] performed experiments on a catenary and a lazy-wave power cable configuration connected to a WEC in shallow water depths. They concluded that the lazy-wave configuration is more suitable for their application because the buoyancy module section decoupled the motions of the WEC from the TDP and reduced the hang-off tensions in the power cable compared with the catenary configuration.

An integrated optimization approach was developed by Yang et al. [14], taking into account the cross-section and overall structural response of a lazy-wave umbilical arrangement connected to an FPSO in a water depth of 800 m. Their optimized design showed a considerably longer fatigue life compared to the initial design. Rentschler et al. [15] presented a genetic optimization approach that changes the location of the buoyancy sections on a power cable. Lazy-wave-shaped power cables connected to a FOWT at shallow and intermediate water depths were optimized regarding the impact on tension, curvature, and fatigue. The resulting configurations had less buoyancy attached and a longer fatigue life than their first designs. Chen et al. [16] used a surrogate model to study the optimization design of a riser in a steep wave configuration in very shallow water. Their method resulted in an optimized riser design. Poirette et al. [17] applied a derivative-free trust region optimization method extended to nonlinearly constrained problems to minimize the capital costs of lazy-wave power cable configurations. Two different cable configurations with similar total costs but different cost distributions were obtained starting from two different initial points. Fylling and Berthelsen [18] showed an optimization procedure using the gradient-based NLPQL program considering the spar buoy, mooring system, and power cable simultaneously. They obtained setups with lower costs than their initial setups. Due to the method, they remark that only local minima might have been found.

The objective of the present study is to optimize a tethered lazy-wave power cable configuration connected to a FOWT in deep water. The optimization procedure is fast and easy to implement in the design process. It is for implementation at the early design stages when the detailed costs of the components are not yet known. The aim is to minimize the total cable length, which typically represents the largest portion of the capital cost [19]. Minimizing the cable distance will also decrease electrical energy losses due to a shorter transmission distance. The SLSQP gradient-based algorithm is applied, which is a novel approach to power cable configuration design to the authors' knowledge. The optimization process uses results obtained from steady-state analyses of power-cable configurations connected to a spar-FOWT.

This work is organized as follows. Section 2 describes the setup of the FOWT and the power cable configuration. Section 3 describes the applied environmental parameters. Section 4 describes the applied optimization procedure. The results are presented and discussed in Section 5. Conclusions are drawn in Section 6.

2. NUMERICAL MODEL SETUP

This section shows the setup of a tethered lazy-wave power cable configuration connecting a FOWT with the seabed in the numerical software OrcaFlex version 11.3d [20]. The present study uses the 5MW OC3-Hywind reference spar-FOWT described by Jonkmann et al. [21,22]. Figure 1 shows the geometry, and Table 1 provides further specifications. The horizontal wind turbine has a rotor diameter of 126.0 m and a hub height of 87.6 m. The spar platform extends 120 m below the still water level (SWL). Schnepf et al. [19,23] provide further details on the numerical model of the FOWT.

TABLE 1: OC3-HYWIND FOWT SPECIFICATIONS [21,22]

Rotor orientation, configuration	-	Upwind, 3 blades
Diameter rotor, hub	*m*	126.0, 3.0
Cut-in, rated, cut-out wind speed	*m/s*	3.0, 11.4, 25.0
Cut-in, rated rotor speed	*rpm*	6.9, 12.1
Rotor, nacelle mass	*t*	110.0, 240.0
Tower, platform mass	*t*	347.46, 7466.33
Center of gravity (COG) below still water level (SWL)	*m*	89.9
Fairlead from centerline	*m*	5.2
Number of mooring lines	-	3
Angle between mooring lines	*deg*	120
Water depth	*m*	320

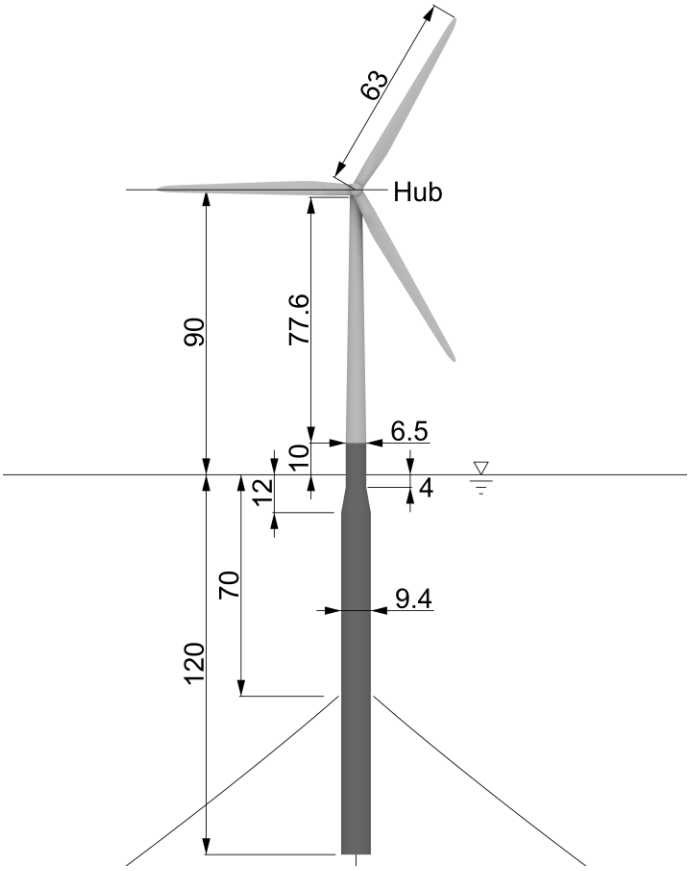

FIGURE 1: OC3-HYWIND FOWT GEOMETRY IN *meters* (TAKEN FROM [23])

The properties of the used 66 kV power cable from Nexans [24] are presented in Table 2. Its setup in a tethered lazy-wave configuration attached to the FOWT is shown in Figure 2, where the power cable is marked in red and the buoyancy section in blue. The properties of the buoyancy section are shown in Table 3. It represents the power cable with commonly available buoyancy modules [25] attached at a center-to-center distance of 2 m. The hang-off location of the power cable is 4.95 m from the vertical spar centerline and 56.4 m above the spar bottom. This location is chosen to avoid excessive marine growth on the power cable at the hang-off. The anchor position of the power cable is 600 m from the vertical spar centerline on the seabed. The entire power cable is placed 60 deg from the adjacent mooring lines. The discretization of the power cable in its initial configurations is presented in Table 4. The entire power cable length of both initial configurations is 690 m. A tether is anchored 452 m from the vertical spar centerline on the seabed. It has a length of 7.0 m and a stiffness of 10 MN. The tether is connected to the power cable with a clamp that has a stiffness of 10 MN. To prevent overbending, bend stiffeners with properties shown in Table 5 and Figure 3 are installed next to the tether clamp.

TABLE 2: POWER CABLE PROPERTIES [24,26]

Core main material	–	Copper
Voltage rating	*kV*	66
Outer diameter	*m*	0.116
Weight in air	*kg/m*	25.0
Torsional stiffness	kNm^2	38.0
Axial stiffness	*MN*	362.0
Bending stiffness, slip	kNm^2	2.4
Tension at conductor yield	*kN*	885.0
Safe handling load	*kN*	531.0
Minimum bending radius	*m*	1.8
Drag coefficient normal	–	1.2
Drag coefficient axial	–	0.008
Added mass coefficient normal	–	1.0
Added mass coefficient axial	–	0.0
Seabed friction coefficient	–	0.5

TABLE 3: BUOYANCY SECTION PROPERTIES

Outer diameter	*m*	0.361
Weight in air	*kg/m*	59.0
Torsional stiffness	kNm^2	38.0
Axial stiffness	*MN*	362.0
Bending stiffness, slip	kNm^2	2.4
Drag coefficient normal	–	2.617
Drag coefficient axial	–	0.345
Added mass coefficient normal	–	1.0
Added mass coefficient axial	–	0.469

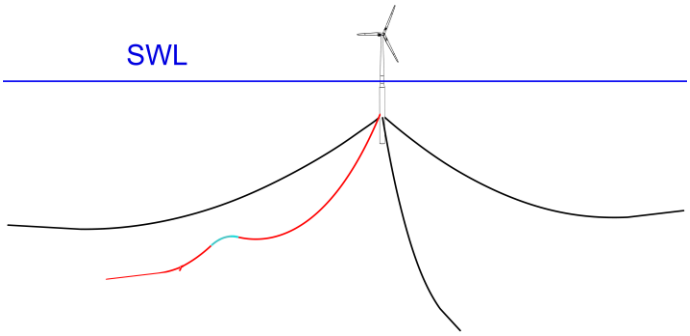

FIGURE 2: SETUP OF THE FOWT WITH THE TETHERED LAZY-WAVE POWER CABLE

TABLE 4: POWER CABLE DISCRETIZATION OF THE INITIAL CONFIGURATIONS

Section description	Section length (m) Case 1	Section length (m) Case 2	Target segment length (m)
Hang-off section	10.00	10.00	0.10
Section 1: L_1	340.00	430.00	1.00
Buoyancy section: L_{BS}	80.00	80.00	0.30
Section 2: L_2	100.00	10.00	1.00
Section 3	6.78	6.78	0.31
Bend stiffener	3.12	3.12	0.12
Tether clamp	0.20	0.20	0.10
Bend stiffener	3.12	3.12	0.12
Section with TDP	65.00	65.00	0.31
Section on the seabed	81.78	81.78	1.00

TABLE 5: BEND STIFFENER PROPERTIES [27]

Diameter	m	0.49 to 0.19
Length	m	2.88
Drag coefficient lateral	$-$	1.1
Added mass coefficient lateral	$-$	1.0

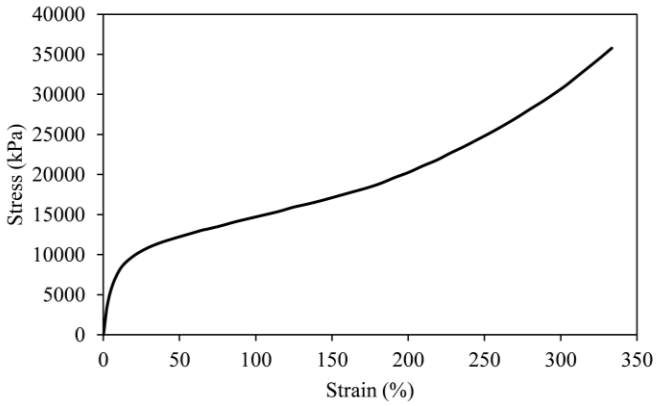

FIGURE 3: STRESS-STRAIN RELATIONSHIP OF THE BEND STIFFENER (REPRODUCED FROM [27])

3. ENVIRONMENTAL CONDITIONS

Four different environmental load cases shown in Table 6 are used in the present study. The two rated load cases have wind speeds in the operation and production regime of the wind turbine. The rated load case A is taken from Jonkman and Musial [28]. The second rated load case B is taken from a location in the northern North Sea with a water depth of 320 m by Asplin et al. [29], Papadopoulos et al. [30], and Spyrou et al. [31]. The same location and sources are used for extreme load case A. The extreme load case B is from Kvitrud and Løland [32], who did measurements at the Visund field in the northern North Sea. The two extreme load cases have wind speeds that exceed the operational range of the wind turbine, causing it to idle.

The Norwegian Petroleum Directorate (NPD) spectrum is the applied wind spectrum [20]. Kvitrud and Løland did not specify the height at which their wind speed measurements were taken, so a standard height of 10 m is assumed. The current velocity is estimated through the power law profile given by DNV [33]. The applied wave spectrum is the Torsethaugen spectrum [20] for the load cases from Asplin et al. [29], Papadopoulos et al. [30], and Spyrou et al. [31]. The JONSWAP spectrum [20] is applied for the other two load cases.

TABLE 6: ENVIRONMENTAL LOAD CASES

Environmental parameter			Rated A [28]	Rated B [29–31]	Extreme A [29–31]	Extreme B [32]
Wind speed	U_{10}	m/s	9.53	3.2	23.66	29.0
Significant wave height	H_s	m	6.0	1.2	11.9	13.2
Spectral peak period	T_p	s	9.93	8.3	13.8	15.1
Peak enhancement factor	γ	$-$	2.872	-	-	2.639
Current at surface	c_s	m/s	0.486	0.06	0.47	1.07

The paper considers three loading directions towards the model, with angles of 0, 90, and 180 deg, to evaluate the most crucial effects of static load. These directions are shown in Figure 4. The 0 deg load represents the near condition, where the FOWT moves towards the TDP due to the applied load. This condition is crucial to ensure compliance with the minimum bending radius requirement for the configuration, as small cable bending radii may occur at the cable section near the TDP and the tether. The 180 deg far condition results from the opposite load direction of the near condition. It causes the FOWT to move away from the TDP, stretching the cable and potentially causing excessive tension. The transverse load is applied 90 deg towards the model, which can cause large hang-off angles and horizontal motion of the power cable. This is due to the current acting on a larger projected area of the cable compared to the in-line near and far conditions. The angle must be such that it guarantees a feasible hang-off section design and the required fatigue life of the cable configuration. Wind, waves, and current are applied in the same direction toward the model in each load case to obtain conservative results.

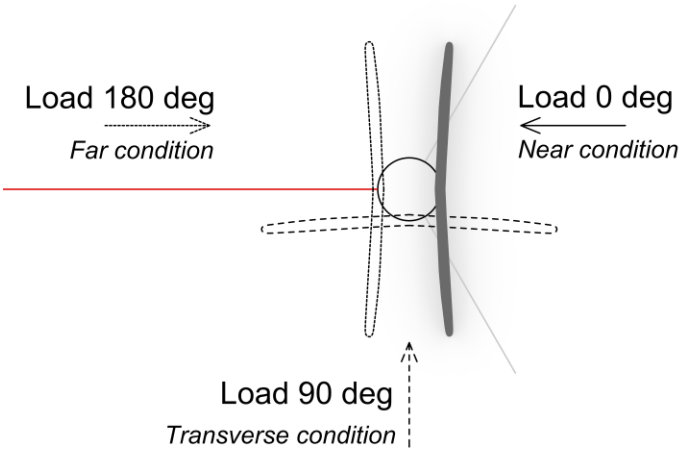

FIGURE 4: ENVIRONMENTAL LOADING DIRECTIONS

4. OPTIMIZATION PROCEDURE

The optimization procedure for the tethered lazy-wave configuration is presented in this section. The present study uses the programming language Python 3.8.7 [34] with the SciPy package version 1.9.3 [35] for optimization. The Sequential Least Squares Programming (SLSQP) algorithm from SciPy is applied. It is a gradient-based numerical optimization algorithm designed to solve constrained optimization problems. The algorithm is capable of handling both equality and inequality constraints. SLSQP relies on analytical gradients of the objective function and constraints to search for the optimal solution. It iteratively improves the initial guess to reduce the objective function through a series of sequential quadratic programming sub-problems. The SLSQP algorithm is categorized as a Sequential Quadratic Programming (SQP) method, meaning that it transforms the initial problem into a series of quadratic programming problems. These are constructed using second-order approximations of the Lagrangian, and the original constraints are linearized and included as constraints.

The algorithm is implemented as provided by SciPy, using the default values of 2^{-24} for the step size used in the finite difference calculation of gradients and 10^{-6} for the precision goal of the result of the objective function.

The objective function to minimize is the total cable length L_{Total} of the tethered lazy-wave configuration:

$$L_{Total} = L_1 + L_{BS} + L_2 + L_{Res} \quad (1)$$

where L_{Res} is the residual length of all sections not included in the optimization.

The design variables or parameters and their admissible domains are defined by:

- Section 1: $50 \text{ m} \leq L_1 \leq 450 \text{ m}$
- Buoyancy section: $10 \text{ m} \leq L_{BS} \leq 200 \text{ m}$
- Section 2: $10 \text{ m} \leq L_2 \leq 200 \text{ m}$

The optimization problem requires additional constraints for the design solution to be functional. All applied constraints in this study are inequality constraints. They are formulated as a set of functions g_i that must be positive values in the solution.

Dynamic amplification factors are implemented for most constraints to account for the difference between the results of the steady-state analyses and the dynamic analyses. Steady-state and dynamic simulations of the initial configurations are carried out. Each environmental load case is simulated with ten different seeds, from which the most extreme responses are extracted. A simulation time of 3 hours is used for each simulation, with a time step of 0.1 s. The constraint values are reduced or increased according to the percentage change from the steady-state to the dynamic simulation results of the initial configurations. These dynamic amplification factors are a safety so that the final configuration will not exceed the design constraints of the model in dynamic analyses.

The solution of the optimization algorithm must respect the following inequality constraints:

- The maximum cable tension $\sigma_{c,max}$ must be smaller than the maximum allowable cable tension $\sigma_{c,lim} = 531.0$ kN:

$$g_1 = 0.20\, \sigma_{c,lim} - \sigma_{c,max} \quad (2)$$

- The cable minimum bending radius $B_{r,min}$ must be larger than the minimum allowable bending radius $B_{r,lim} = 1.8$ m. A safety factor is applied to account for future design near and far conditions:

$$g_2 = 1.48\, B_{r,lim} - B_{r,min} \quad (3)$$

- The tether tension $\sigma_{t,max}$ must be smaller than the maximum allowable tether tension $\sigma_{t,lim} = 60$ kN:

$$g_3 = 0.5\, \sigma_{t,lim} - \sigma_{t,max} \quad (4)$$

- The hang-off angle α must not exceed the imaginary line between the hang-off location and tether to avoid an expensive hang-off section design. The limiting angle in this setup is $\alpha_{lim} = 63$ deg from the vertical spar axis. A safety factor is applied for future near and far conditions:

$$g_4 = \alpha_{lim} - \alpha \quad (5)$$

- The hang-off angle β must not exceed the limiting value of hang-off angle α in the horizontal direction to avoid an expensive hang-off section design. The limiting angle in this setup is $\beta_{lim} = 63/2$ deg from the imaginary line between the hang-off location and tether in the horizontal direction:

$$g_5 = \beta_{lim} - |\beta| \quad (6)$$

- A minimum seabed clearance must be guaranteed for the power cable section between the hang-off and the tether. The minimum seabed clearance is $z_{lim} = 10$ m:

$$g_6 = z_{min} - z_{lim} \tag{7}$$

A constraint to guarantee a clearance between the power cable and the sea surface is not implemented. The vertical cable excursion within the given bounds never exceeds the hang-off location.

The extreme environmental loading condition B is used in the optimization algorithm. It showed the most critical responses in the steady-state and dynamic simulations of the initial configurations with the four environmental load cases. Its steady state is calculated separately for each of the three loading directions at each optimization step.

The numerical model provided as input to the optimization algorithm needs to be suited for steady-state analysis. Dynamic analysis is not required; hence the model can be preliminary, such as at the start of the design process. Apart from the numerical model, the bounds of the section lengths and the limiting values for the constraints must be known.

5. RESULTS AND DISCUSSION

This section presents the results of the optimizations and discusses them. Two optimization types of the tethered lazy-wave configuration are carried out. First, only two optimization parameters are considered. Second, three optimization parameters are taken into account by the algorithm.

The buoyancy section length and location are varied in the first optimization with two parameters. The lengths of Section 1 and Section 2 can be varied, but they always have a total length of 440 m. This moves the location of the buoyancy section.
The optimization algorithm converged to an overall cable length of 672.3 m, which is a reduction of 2.6% compared with the initial design. The buoyancy section has a length of 62.3 m, and its center is located at 355.1 m from the hang-off along the cable length. The convergence of the parameters in the optimization is shown in Figure 5. Figure 6 shows the obtained constraint parameters normalized by the constraint values at each simulation step. The optimization runtime for the presented results is 37 min. The convergence to the solution can be observed in the results past 226 iterations, where the variables come close to a straight line in the plots.

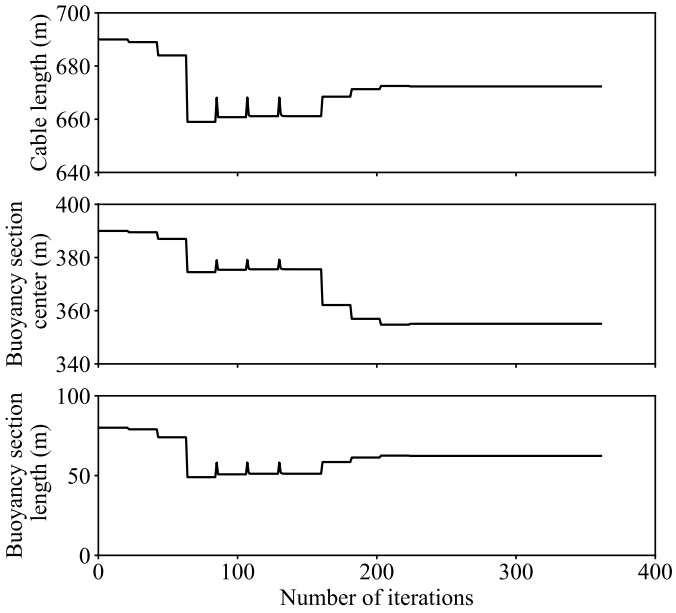

FIGURE 5: PARAMETER CONVERGENCE IN THE OPTIMIZATION PROCESS WITH 2 PARAMETERS

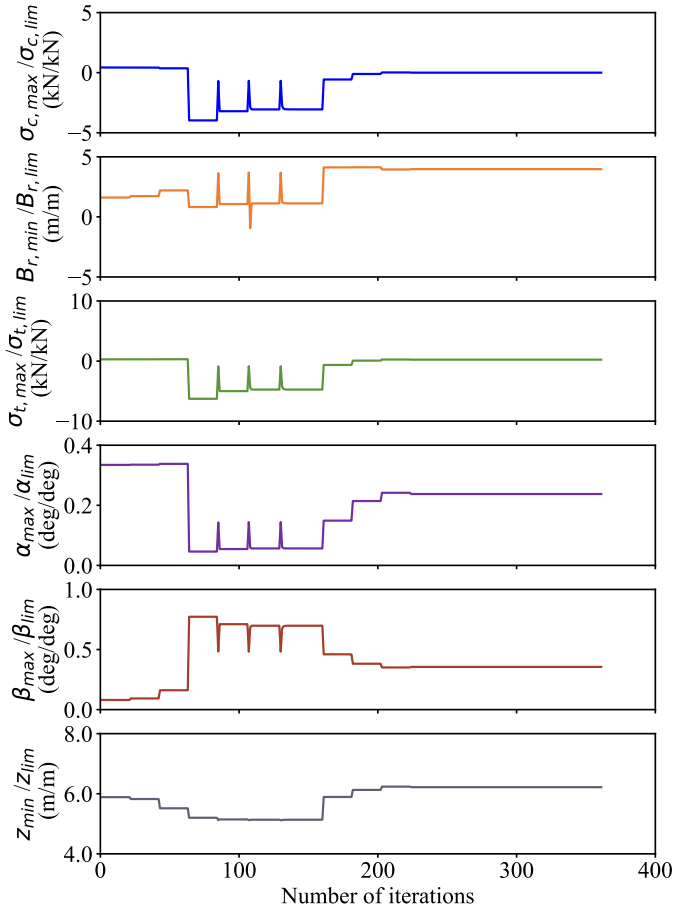

FIGURE 6: CONSTRAINT PARAMETERS CONVERGENCE IN THE OPTIMIZATION PROCESS WITH 2 PARAMETERS

A brute force method is used to confirm the obtained solution of the two-parameter optimization. Steady-state analyses are conducted with all tethered lazy-wave setups within the specified bounds of the buoyancy section length and location. Figure 7 shows the resulting design space filled in grey. The constraint lines plotted in the figure surround the configurations so that they are included in or excluded from the design space due to their constraint criterion. The optimization algorithm has successfully converged to a minimum global solution within the design space. As the buoyancy section length is minimum in the solution, the cable length is also minimum in the two-parameter optimization. It shows that the algorithm optimized the power cable configuration successfully.

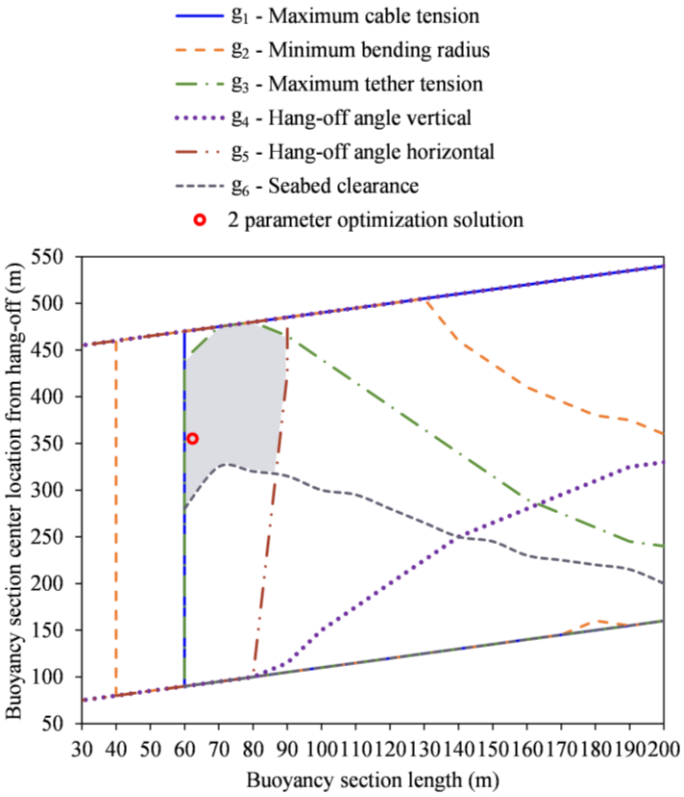

FIGURE 7: CONSTRAINT CRITERIONS FRAMING THE DESIGN SPACE IN THE 2-PARAMETER OPTIMIZATION

In the second optimization type, three parameters are varied: The lengths of Section 1, the buoyancy section, and Section 2. Two different starting points for the optimization are chosen. Case 1 has the buoyancy section implemented closer to the hang-off than Case 2 in the initial configuration. Case 2 has the buoyancy section located close to the tether in the initial configuration.

Figures 8 and 9 show the convergence of the parameters and normalized constraint parameters in the second optimization for Case 1. Figures 10 and 11 show the convergence likewise for Case 2. Convergence can be observed from an iteration number of 229 for Case 1 and 390 for Case 2. The solution converges significantly earlier for Case 1 than for Case 2. This is because the solution in Case 2 is significantly different than in Case 1 compared to their initial configurations.

The optimization runtime is 37 min for the optimization with three variables in Case 2. However, convergence has already been obtained much earlier than in the presented result. For Case 1, the runtime is 71 min for the presented results, which is longer than for Case 2. Figures 8 and 10 show that the convergence for Case 1 is already achieved at an earlier iteration number than for Case 2. The algorithm could have been terminated earlier after convergence to decrease the runtime. Increasing the step size in the finite difference calculation of the gradients can also lead to a faster result. The acquired runtime is short enough to use the tool to design power cable configurations.

The fluctuations in variable parameters during optimization deviate from the anticipated smoothness that characterizes gradient-based approaches. This deviation may suggest that the objective function is not entirely smooth, thereby calling for alternative optimization strategies to be considered. Similar irregularities in the variable parameter changes can be observed in the two-parameter optimization. However, the brute force method results show that the optimization algorithm converged to the minimum solution.

In the three-parameter optimization, the resulting overall power cable length is 672.8 m for both cases. It is a reduction of 2.6% in cable length compared to the initial design. The reduction can be more significant with initial configurations that have longer cables. Table 7 shows the optimized cable section discretization. Case 1 and Case 2 have only slightly different lengths for the buoyancy section and Section 2. The similarities in the resulting configurations indicate that both solutions are very close to a global minimum. This shows that the gradient-based method can be applied in the design process of power cable configurations in marine environments.

TABLE 7: POWER CABLE DISCRETIZATION OF THE OPTIMIZED CONFIGURATIONS

Section description	Section length (m) Case 1	Section length (m) Case 2	Section length (m) 2 parameters
Hang-off section	10.00	10.00	10.00
Section 1: L_1	333.89	332.79	313.92
Buoyancy section: L_{BS}	73.42	69.87	62.33
Section 2: L_2	95.50	100.14	126.08
Section 3	6.78	6.78	6.78
Bend stiffener	3.12	3.12	3.12
Tether clamp	0.20	0.20	0.20
Bend stiffener	3.12	3.12	3.12
Section with TDP	65.00	65.00	65.00
Section on the seabed	81.78	81.78	81.78

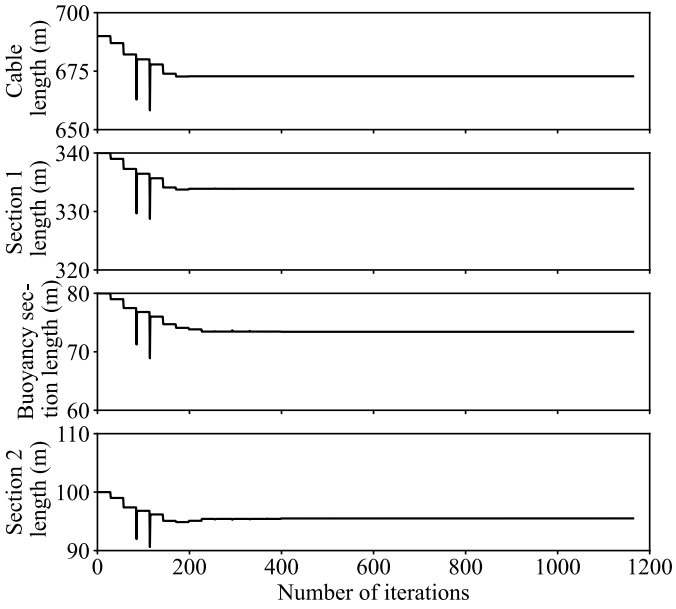

FIGURE 8: PARAMETER CONVERGENCE IN THE OPTIMIZATION PROCESS WITH 3 PARAMETERS, CASE 1

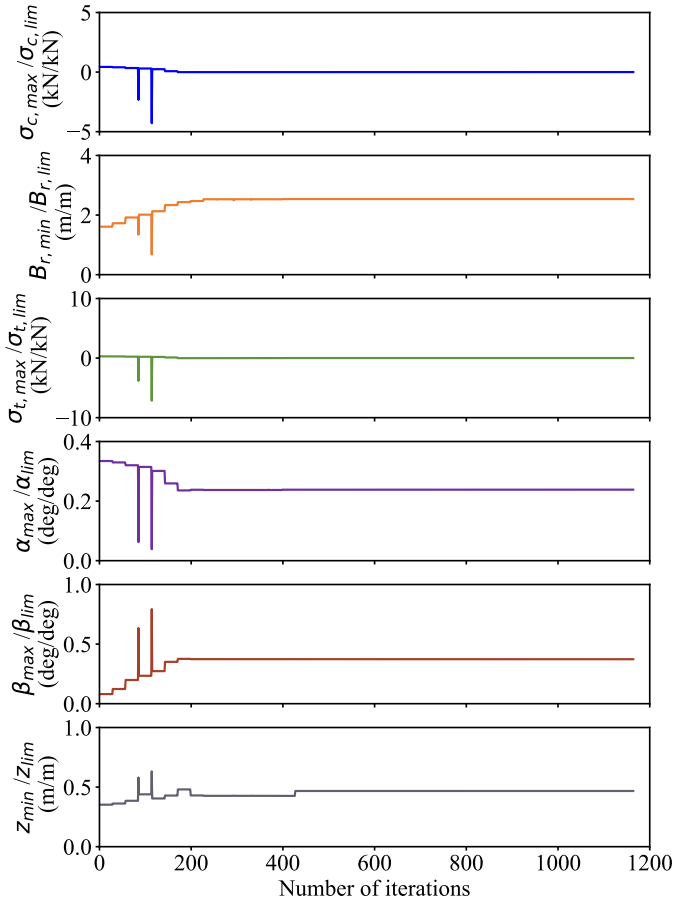

FIGURE 9: CONSTRAINT PARAMETERS CONVERGENCE IN THE OPTIMIZATION PROCESS WITH 3 PARAMETERS, CASE 1

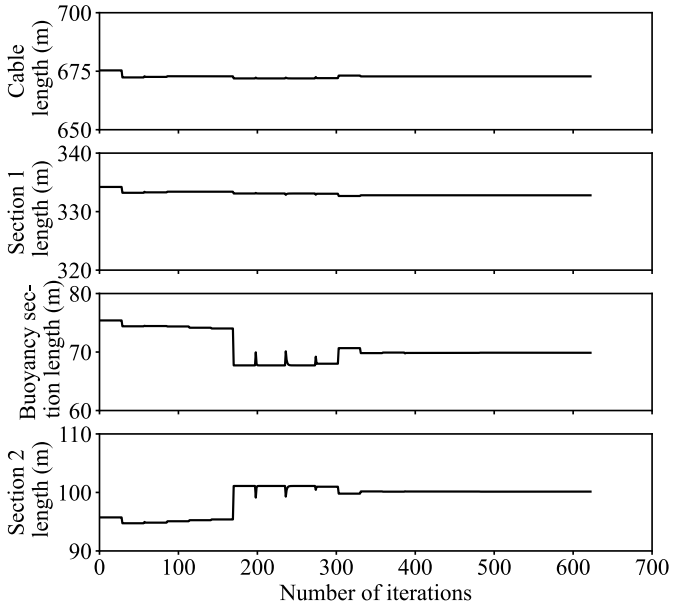

FIGURE 10: PARAMETER CONVERGENCE IN THE OPTIMIZATION PROCESS WITH 3 PARAMETERS, CASE 2

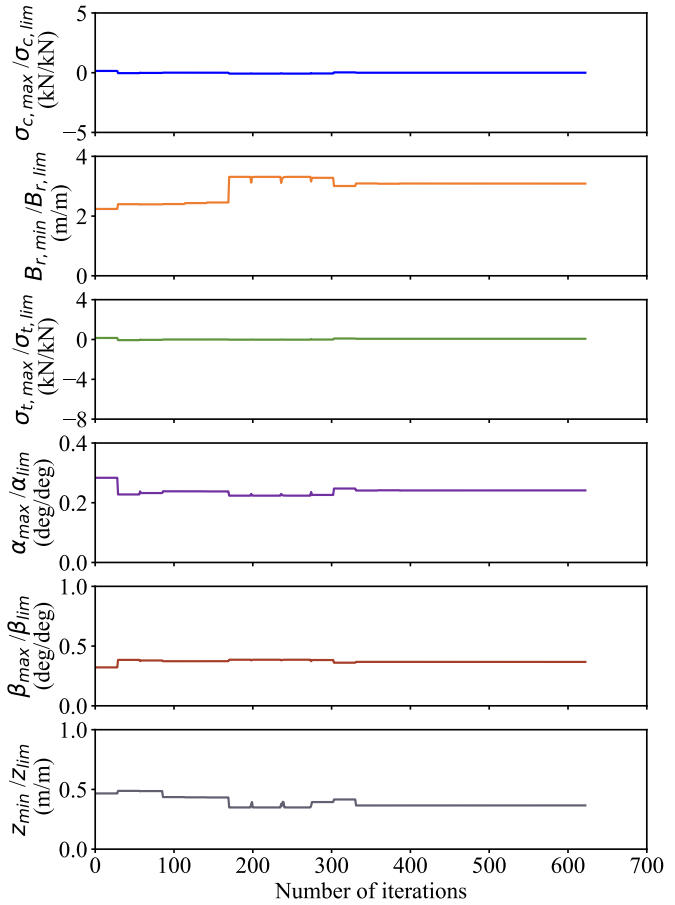

FIGURE 11: CONSTRAINT PARAMETERS CONVERGENCE IN THE OPTIMIZATION PROCESS WITH 3 PARAMETERS, CASE 2

Figure 12 shows the resulting static geometries of the cable configurations without applied environmental loads. The configuration obtained from the optimization with three parameters results in a standard tethered lazy-wave shape with a shorter cable length than the initial design. The presented result is the configuration obtained for Case 1, but the resulting configuration for Case 2 is similar. The configuration obtained from the optimization with two parameters has a shorter buoyancy section than the other configurations, resulting in the flattest out of the three configurations. The optimization with three parameters is more suitable for tethered lazy-wave power cable configurations than with two parameters.

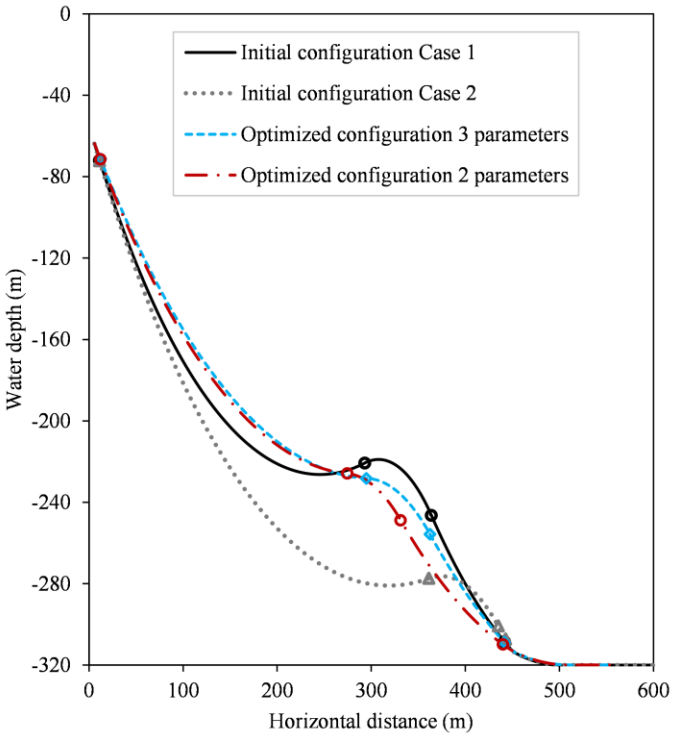

FIGURE 12: STATIC GEOMETRIES OF THE CABLE CONFIGURATIONS

Dynamic analyses of the optimized configuration with three parameters are carried out. Each environmental load case is simulated with ten different seeds, from which the most extreme responses are extracted. A simulation time of 3 hours is used for each simulation, with a time step of 0.1 s. Table 8 shows the results from the dynamic simulations. All results obey the limiting values for the constraints. This indicates that using the dynamic amplification factors is sufficient for the optimization.
The maximum effective cable tensions in all load cases are at their lowest in the near condition but highest in the far condition. It indicates that the motion and displacement of the floater have a substantial effect on the cable. The increase in maximum tension can also be observed for the far condition of the tether compared to the near condition. In the far condition, the power cable is pulled away from the tether on the seabed leading to increased maximum tensions.
The vertical maximum hang-off angle of the power cable is at its lowest for the near conditions when the FOWT is closest to the TDP. Conversely, the most significant angles are observed for the far conditions. Transverse load cases increase the maximum horizontal hang-off angles. In these cases, the current load is applied to the largest projected area of the cable, causing it to deflect sideways. As a result, the maximum effective cable tensions of the transverse load case are larger than in the near condition but smaller than in the far condition.

TABLE 8: DYNAMIC ANALYSIS RESULTS FROM THE 3-PARAMETER OPTIMIZED CONFIGURATION, CASE 1.

		Rated A	Rated B [29–31]	Extreme A	Extreme B
Maximum effective cable tension					
Near	*kN*	53.7	61.6	79.3	70.1
Transverse	*kN*	65.6	63.5	77.3	120.9
Far	*kN*	263.9	70.0	305.8	350.9
Minimum cable bending radius					
Near	*m*	12.3	14.5	9.2	6.1
Transverse	*m*	12.8	14.7	12.0	8.5
Far	*m*	6.6	14.5	8.0	7.9
Maximum tether tension					
Near	*kN*	11.2	13.2	25.1	25.1
Transverse	*kN*	15.8	14.0	21.8	50.4
Far	*kN*	52.8	16.6	50.8	58.4
Vertical maximum hang-off angle					
Near	*deg*	32.5	38.5	26.3	31.7
Transverse	*deg*	37.6	39.5	37.0	39.3
Far	*deg*	45.7	39.9	42.5	50.3
Horizontal maximum hang-off angle					
Near	*deg*	1.1	0.1	0.4	0.5
Transverse	*deg*	1.2	0.2	3.8	7.8
Far	*deg*	1.7	0.1	0.1	0.3
Cable seabed clearance between FOWT and tether					
Near	*m*	11.3	11.1	10.4	11.8
Transverse	*m*	10.6	11.1	10.3	10.1
Far	*m*	10.6	11.0	11.7	12.0
Cable sea surface clearance					
Near	*m*	62.6	63.7	59.6	59.7
Transverse	*m*	61.9	63.6	59.7	59.8
Far	*m*	62.6	63.6	59.8	59.5

6. CONCLUSION

The present work introduces a gradient-based optimization algorithm for tethered lazy-wave power cable configurations. The optimization method applied is SLSQP with two and three design variables. The design variables are different section lengths of the cable, including the buoyancy section. The constraints are the maximum effective tension of the power

cable, the minimum bending radius, the vertical and horizontal hang-off angles, the tension in the tether near the TDP, and the minimum seabed clearance. Steady-state environmental loads are applied in three directions on the model in the optimization process. Different initial configurations have been chosen as starting points for the optimization. The algorithm converges to a minimized solution within the design criteria in all applications. The resulting power cable configurations from the different initial configurations are similar, indicating that a global minimum has been found. The resulting configurations show a 2.6% shorter cable length than the initial design, as the cable length of the initial design is close to the optimum length. It shows that the gradient-based optimization approach can be used in the design process of tethered lazy-wave power cable configurations.

Further work will extend the optimization procedure to continuing stages of the design process. This will include more design variables in the optimization procedure, such as the locations of the hang-off and TDP, as well as installation tolerances of the tether anchor on the seabed. Apart from static and steady-state simulations, this work will be extended to dynamic analysis and the integration of marine growth and fatigue analysis in the procedure.

ACKNOWLEDGEMENTS

This research is funded by the Research Council of Norway (project number 320902). The authors would like to thank Nexans Norway AS for providing the properties of the power cable used in the present study.

REFERENCES

[1] Carbon Trust, 2021, "Cable Burial Risk Assessment (CBRA) Guidance and Application Guide" [Online]. Available: https://www.carbontrust.com/de/node/1321. [Accessed: 23-Sep-2021].

[2] Eldøy, S., Vold, O., Graven, H., Guttormsen, T., and Delp, L., 2017, *Hywind Scotland Pilot Park Project Plan for Construction Activities 2017*, C178-HYS-Z-GA-00001, Statoil, Norway.

[3] Duarte, T. M., 2021, "WindFloat Atlantic Project - A Step Change towards Commercial Floating Wind."

[4] Equinor, 2019, *Hywind Tampen, PL050 - PL057 - PL089, PUD del II - Konsekvensutredning*, Norway.

[5] Rentschler, M. U. T., Adam, F., Chainho, P., Krügel, K., and Vicente, P. C., 2020, "Parametric Study of Dynamic Inter-Array Cable Systems for Floating Offshore Wind Turbines," Marine Systems & Ocean Technology, **15**(1), pp. 16–25.

[6] Zhao, S., Cheng, Y., Chen, P., Nie, Y., and Fan, K., 2021, "A Comparison of Two Dynamic Power Cable Configurations for a Floating Offshore Wind Turbine in Shallow Water," AIP Advances, **11**(3), p. 035302.

[7] Ikhennicheu, M., Lynch, M., Doole, S., Borisade, F., Wendt, F., Schwarzkopf, M.-A., Matha, D., Vicente, R. D., Tim, H., Ramirez, L., and Potestio, S., 2020, *Review of the State of the Art of Dynamic Cable System Design*, D3.1, corewind, EU.

[8] Ottesen, T., 2010, "Extreme Response Estimation of Umbilical on Very Deep Water," Master's Thesis, Norwegian University of Science and Technology.

[9] Hall, M., Sirnivas, S., and Yu, Y.-H., 2021, "Implementation and Verification of Cable Bending Stiffness in MoorDyn," *ASME 2021 3rd International Offshore Wind Technical Conference*, American Society of Mechanical Engineers, Virtual, Online.

[10] Nicholls-Lee, R., Thies, P. R., and Johanning, L., 2021, "Coupled Global-Local Modelling for Dynamic Submarine Power Cables," ORE.

[11] Thies, P. R., Johanning, L., and Dobral, C., 2017, "Parametric Sensitivity Study of Submarine Power Cable Design for Marine Renewable Energy Applications," *Proceedings of the ASME 2017 36th International Conference on Ocean, Offshore and Arctic Engineering*, American Society of Mechanical Engineers, Trondheim, Norway.

[12] Thies, P. R., Johanning, L., and Smith, G. H., 2011, "Assessing Mechanical Loading Regimes and Fatigue Life of Marine Power Cables in Marine Energy Applications," Proceedings of the Institution of Mechanical Engineers, Part O: Journal of Risk and Reliability, **226**(1), pp. 18–32.

[13] Martinelli, L., Lamberti, A., Ruol, P., Ricci, P., Kirrane, P., Fenton, C., and Johanning, L., 2010, "Power Umbilical for Ocean Renewable Energy Systems - Feasibility and Dynamic Response Analysis," p. 8.

[14] Yang, Z., Yan, J., Sævik, S., Lu, Q., Ye, N., Chen, J., and Yue, Q., 2021, "Integrated Optimisation Design of a Dynamic Umbilical Based on an Approximate Model," Marine Structures, **78**, p. 102995.

[15] Rentschler, M. U. T., Adam, F., and Chainho, P., 2019, "Design Optimization of Dynamic Inter-Array Cable Systems for Floating Offshore Wind Turbines," Renewable and Sustainable Energy Reviews, **111**, pp. 622–635.

[16] Chen, J., Yan, J., Yang, Z., Yue, Q., and Tang, M., 2016, "Flexible Riser Configuration Design for Extremely Shallow Water With Surrogate-Model-Based Optimization," Journal of Offshore Mechanics and Arctic Engineering, **138**(4), p. 041701.

[17] Poirette, Y., Guiton, M., Huwart, G., Sinoquet, D., and Leroy, J. M., 2017, "An Optimization Method for the Configuration of Inter Array Cables for Floating Offshore Wind Farm," *Volume 10: Ocean Renewable Energy*, American Society of Mechanical Engineers, Trondheim, Norway.

[18] Fylling, I., and Berthelsen, P. A., 2011, "WINDOPT: An Optimization Tool for Floating Support Structures for Deep Water Wind Turbines," *Volume 5: Ocean Space Utilization; Ocean Renewable Energy*, ASMEDC, Rotterdam, The Netherlands, pp. 767–776.

[19] Schnepf, A., Lopez-Pavon, C., Ong, M. C., Yin, G., and Johnsen, Ø., 2023, "Feasibility Study on Suspended Inter-Array Power Cables Between Two Spar-Type Offshore Wind Turbines," Ocean Eng., (VSI: Marine operations).

[20] Orcina Ltd, 2023, “OrcaFlex” [Online]. Available: https://www.orcina.com/webhelp/OrcaFlex/. [Accessed: 05-Jan-2023].
[21] Jonkman, J., Butterfield, S., Musial, W., and Scott, G., 2009, *Definition of a 5-MW Reference Wind Turbine for Offshore System Development*, NREL/TP-500-38060, National Renewable Energy Laboratory, Golden, CO, United States.
[22] Jonkman, J., 2010, *Definition of the Floating System for Phase IV of OC3*, NREL/TP-500-47535, National Renewable Energy Laboratory, Golden, CO, United States.
[23] Schnepf, A., Devulder, A., Johnson, Ø., Ong, M. C., and Lopez-Pavon, C., 2023, “Numerical Investigations on Suspended Power Cable Configurations for Floating Offshore Wind Turbines in Deep Water Powering an FPSO,” J. Offshore Mech. Arct. Eng., **145**(3).
[24] Nexans Norway AS, 2022, *Technical Description - Subsea Composite Cable*, OM1052.
[25] PartnerPlast AS, 2021, “Offshore & Subsea - Buoyancy Systemes and Cable Protection Solutions.”
[26] NORSOK, 2017, *Actions and Action Effects*, N-003:2017, Norway.
[27] bin Ahmad, I., Schnepf, A., and Ong, M. C., 2023, “An Optimization Methodology for Suspended Inter-Array Power Cable Configurations between Two Floating Offshore Wind Turbines,” Ocean Eng.
[28] Jonkman, J., and Musial, W., 2010, *Offshore Code Comparison Collaboration (OC3) for IEA Task 23 Offshore Wind Technology and Deployment*, NREL/TP-5000-48191, National Renewable Energy Laboratory, Golden, CO, United States.
[29] Asplin, L., Albretsen, J., Johnsen, I. A., and Sandvik, A. D., 2020, “The Hydrodynamic Foundation for Salmon Lice Dispersion Modeling along the Norwegian Coast,” Ocean Dynamics, **70**(8), pp. 1151–1167.
[30] Papadopoulos, A., Nickovic, S., and Missirlis, N., 1997, “The ETA Model Operational Forecasting System and Its Parallel Implementation.”
[31] Spyrou, C., Mitsakou, C., Kallos, G., Louka, P., and Vlastou, G., 2010, “An Improved Limited Area Model for Describing the Dust Cycle in the Atmosphere,” Journal of Geophysical Research, **115**.
[32] Kvitrud, A., and Løland, A. H., 2018, “Observed Wave Actions on Norwegian Semi-Submersible and TLP Decks,” *Volume 1: Offshore Technology*, American Society of Mechanical Engineers, Madrid, Spain, p. V001T01A023.
[33] DNV GL AS, 2019, *Environmental Conditions and Environmental Loads*, DNVGL-RP-C205.
[34] Python Software Foundation, 2023, “Python,” python [Online]. Available: https://www.python.org/. [Accessed: 05-Jan-2023].
[35] The SciPy community, 2023, “Scipy.Optimize.Minimize” [Online]. Available: https://docs.scipy.org/doc/scipy/reference/generated/scipy.optimize.minimize.html. [Accessed: 08-Jan-2023].